Entrainment of Shelf Water by a Bifurcating Continental Boundary Current

MELVIN E. STERN

The Florida State University, Tallahassee, Florida

JAY AUSTIN

MIT–WHOI Joint Program, Woods Hole Oceanographic Institute, Woods Hole, Massachusetts

(Manuscript received 14 September 1994, in final form 2 May 1995)

ABSTRACT

At the northeast corner of Taiwan the direction of the continental slope isobaths changes rapidly relative to the oncoming Kuroshio, so that the inertia of a small inshore fraction of this current causes it to cross the slope, while the main branch follows the isobaths. It is suggested that the portion of the bifurcated current entering the shelf displaces ambient water of relatively high potential vorticity as a countercurrent, which flows across the slope. The vortex stretching and subsequent entrainment of this water into the main branch of the Kuroshio increases its maximum cyclonic vorticity and helps to maintain the inshore shear of the western boundary current. This idea is supported by simple initial value and steady-state models, and also by dye observations of the flow from a source on the wall of a rotating tank.

1. Introduction

The mean path of an inviscid barotropic boundary current depends on its Rossby number and on the variation in bottom depth. When the latter is relatively large, we know that a potential vorticity-conserving current tends to follow curved isobaths, and when it is small the current tends to flow in a straight path. When the two factors are comparable, their competition can result in the current splitting into two branches; one of many examples is the Gulf Stream south of Newfoundland (Warren 1969). More relevant to this study is the Kuroshio at the northeast corner of Taiwan (Hsueh et al. 1992), where the direction of the continental slope isobaths changes rapidly relative to the oncoming western boundary current, so that an inshore portion of this tends to flow across the continental slope and into the East China Sea, where it eventually mixes. The main (offshore) portion of the Kuroshio, however, follows the curved continental slope northeastward.

This type of bifurcation will be studied theoretically and experimentally, with special attention directed to the entrainment of shelf/slope water in the main branch that continues flowing along the continental slope. The vortex stretching involved in this process may be important in generating and maintaining the inshore shear of western boundary currents (Stern 1991), as contrasted with a vorticity *diffusion* process acting at a (hypothetical) no-slip vertical wall (e.g., Munk 1950).

The way in which the entrainment arises will first be illustrated by considering an idealized (but dynamically consistent) initial value problem (Fig. 1) in which an inviscid semi-infinite half jet, containing only *anticyclonic* relative vorticity, is incident on a shallow shelf. As the blunt nose of the vorticity front bounding the intrusion approaches the continental slope, it displaces a countercurrent in the exterior fluid. In the case of a completely flat bottom ($\Delta H = 0$) contour dynamical calculations (Stern and Pratt 1985) show that as this intrusion continues along the wall the nose pinches off, tending to form an eddy with closed vorticity isopleths; and behind this a new nose forms at the leading edge of the wall current. For sufficiently small finite ΔH and Coriolis parameter f, a kinematically similar behavior is expected, modified by a small increase in the anticyclonic vorticity as the current enters the shelf, and by an increase in the near wall velocity. But for larger (f, ΔH) a different and topographically controlled regime is expected, in which only a fraction G of the upstream transport (T_0) enters the shelf, while the remainder ($1 - G$) flows along the slope isobaths. Since the resulting full jet must contain *cyclonic* vorticity and since none of this exists upstream, it somehow must be generated by the displacement of high potential vorticity (f/H) shelf water into the deeper region and subsequent merger of this water with that portion of the upstream anticyclonic wall current that bifurcates before the shelf. The same conclusion holds

Corresponding author address: Prof. Melvin E. Stern, Department of Oceanography, The Florida State University, Tallahassee, FL 32306-3048.
E-mail: stern@ocean.fsu.edu

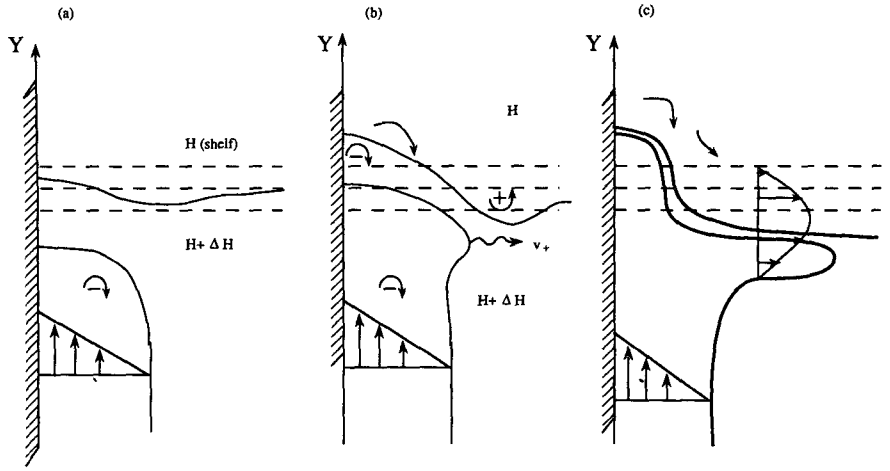

FIG. 1. Illustration of the bifurcation–entrainment mechanism for a barotropic (western) wall current in deep water ($H + \Delta H$) that flows toward a shallow continental slope. (a) The upstream anticyclonic half jet is bounded by a potential vorticity interface, the nose of which is initially far from the slope isobaths (dashed lines). The potential vorticity isolines, initially coincident with the isobaths, are deflected by the approaching nose, as indicated by one of these isolines (the solid curve on the slope). (b) The current flowing along the wall increases its anticyclonic vorticity (as indicated by "−") and increases in speed as it ascends the slope. The compensating offshore displacements generate cyclonic (+) vorticity, which induces a velocity (v_+) on the shear flow interface. (c) A portion of this current can be drawn away from the wall to merge with the entrained "+" fluid to form a free jet, provided ΔH and f are sufficiently large (see text).

even if there is a transverse continental slope in the upstream region of the laminar wall current, and thus we see that entrainment is a *kinematical* necessity if any portion of the half-jet flows along the slope. Note that this entrainment need not occur for all (f, ΔH), since another steady solution might exist in which the entire current adheres to the wall for all y and merely increases its anticyclonic vorticity as it crosses the slope. Such a state is probably unrealizable for large (f, ΔH) if the downstream basin is semienclosed (cf. Fig. 3) with the sink located in the upstream basin.

A more insightful *dynamical* explanation of the bifurcation can be obtained by considering the initial state (Fig. 1) in which the potential vorticity isopleths on the slope are assumed coincident with the isobaths. The deflection of one of the isopleths at a slightly later time (Fig. 1a) is indicated by the solid curve, the inshore portion of which is deflected into the shallow region by the advancing nose, thereby generating anticyclonic (negative) relative vorticity. The opposite deflection of the outer portion of the isopleth generates cyclonic (positive) vorticity, which induces an alongslope velocity v_+ on the upstream vorticity front (Fig. 1b). Depending on f and H, this velocity may be sufficiently large to detach the outer part of the upstream wall current, thereby causing its anticyclonic vorticity to merge with the cyclonic vorticity of the entrained shelf water. The result is a free jet on the slope, containing equal amounts of both vorticities, and flowing away from the wall (Fig. 1c). This mechanistic argument supplements the aforementioned kinematic constraint and leads us to expect that bifurcation with entrainment can occur for a more general upstream jet $U(\xi)$ having cyclonic inshore vorticity. In this case (Fig. 2) the displaced shelf water can increase the maximum cyclonic vorticity on the inshore side of the free jet that follows the continental isobaths, thereby helping to maintain the inshore shear against dissipative influences farther downstream.

These dynamical assertions are testable in the context of an initial value calculation (as subsequently discussed) for an inviscid and piecewise uniform potential vorticity model. Separation from a boundary can occur in such models without allowing velocity discontinuities (vortex sheets), provided the requisite amounts of vorticity are available, as can be seen in the contour dynamical calculation (Stern and Whitehead 1990) of the two-dimensional flow of a jet around a curved wall. But it is important to realize that the separation in that case, as well as the classical (viscous) separation from a nonrotating curved wall, is different from that in Figs. 1, 2, 3. In the former case the *entire* boundary layer is removed from the wall as a result of adverse pressure gradients, flow deceleration, and velocity reversal; in the topographic problem, on the other hand, the inviscid effect accelerates the near-wall velocity (as previously mentioned), and therefore a finite portion of the inshore jet (Fig. 2) remains on the wall, while the rest separates by flowing along the slope topography. The required vorticity comes from vortex stretching rather than viscosity.

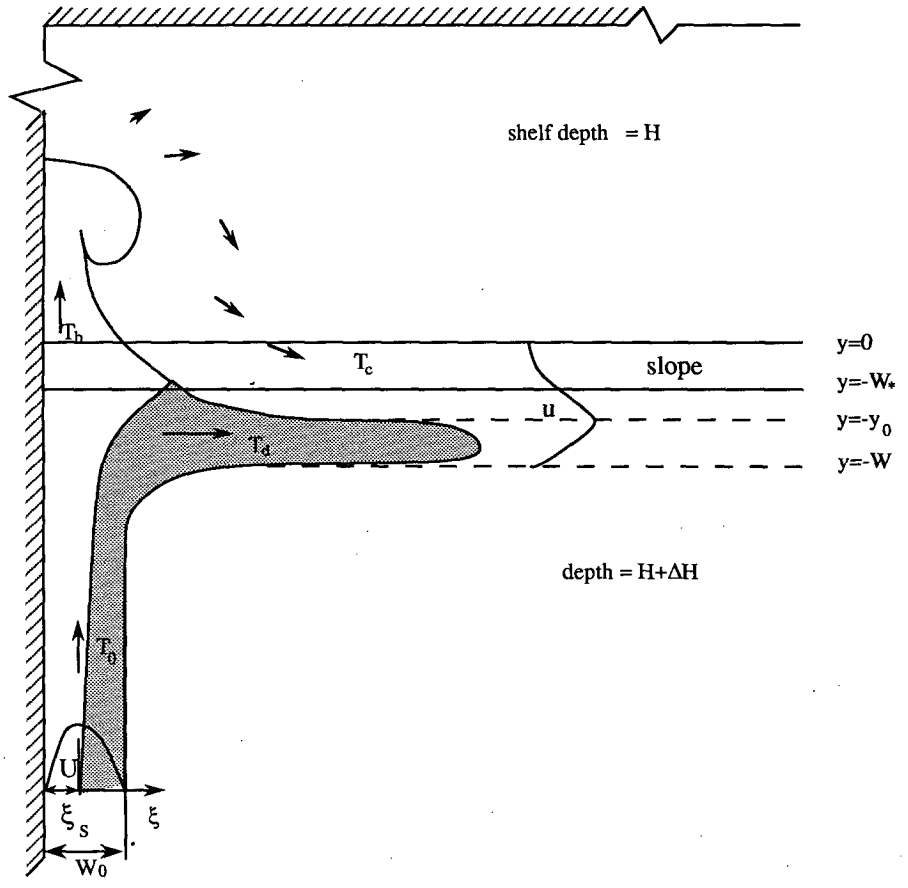

FIG. 2. A more realistic upstream boundary current $U(\xi)$ with transport T_0 flows toward a slope whose depth $h(y)$ increases in the region from $y = 0$ to $y = -W_*$. This slope width is assumed sufficiently narrow so that the bifurcated current (T_d) lies entirely in deep water. The cross-slope flow (T_b) is assumed to displace an equal volume (T_c) of initially resting shelf water as a countercurrent across the slope, where it merges with T_d to form a free jet with velocity $u(y)$ farther downstream. The separating streamline originates at $\xi = \xi_s$ and is at $y = -y_0$ in the free jet. Neither the eastern wall of the semienclosed shelf nor the sink (in deep water) is shown (but see Fig. 3).

The previous initial value arguments do not indicate how a steady narrow countercurrent can be maintained after the nose of the intruding wall current extends far downstream from the slope. Of course, if the downstream basin (Figs. 2, 3) is enclosed on three sides, then the portion (T_b) of $U(\xi)$ that crosses the slope on the wall must at all times produce an equal and opposite cross-slope flow, which exits the upstream basin at some sink (not shown in Fig. 2). But it is not obvious that this counterflow occurs in the vicinity of the bifurcation point (Fig. 2) as a strong narrow current, rather than as a broad weak flow occuring over the entire span of the slope region. This important qualitative assumption will be addressed (section 5) by a laboratory experiment.

In the steady-state theory of section 2 this assumption is made, in addition to the assumption that laminar slope jet $u(y)$ results from the merger of the countercurrent with the bifurcated branch (T_d) of the upstream current (Fig. 2). The two end states can be related by mass and potential vorticity conservation to determine $u(y)$ as a functional of $U(\xi)$, without the need to consider the detailed dynamics of the intervening region where the separation occurs.

Support for the validity and realizability of the main assumption concerning the countercurrent is obtained from a qualitative laboratory experiment (section 5) similar to the one by Spitz and Nof (1990), except that their slope topography consisted of a discontinuous step, while we use a "narrow" slope that is sufficiently wide to justify shallow-water theory, to eliminate free viscous shear layers, and to conserve potential vorticity.

It is convenient to refer to the geometry of the system in Figs. 1 and 2 as "western boundary step-up," since the fluid is assumed to be rotating in the Northern Hemisphere (counterclockwise) sense, and since the bottom elevation increases in the direction of the

boundary current. The dynamical significance of this geometry lies in the fact that the topographic signal wave generated by a current impinging on the slope is directed (westward) *opposite* to $u(y)$. While these waves are not explicit in our steady theory, we believe they may play an important role in obtaining such a state from an initial value problem. [See Johnson's (1985) linear theory for the influence of the topographic Rossby wave direction on the flow from a source to a sink.] The lab experiment requires that the source for producing a wall current be placed on the *eastern* boundary, and therefore a "step down" slope was used to prevent the topographic waves propagating ahead of the (westward flowing) slope current. The theory for this geometry (section 2b) is basically similar to the western boundary case.

The theory of section 2 applies to a continental slope that is sufficiently narrow so that it is entirely crossed by some of the entrained fluid, and the oceanographically interesting case of a "wide" slope is discussed in section 3. Section 4 shows how our theory can be extended to the simplest baroclinic problem, namely a "$1\frac{1}{2}$-layer" density model.

The reader is referred to a review by Ierly (1990) for more general aspects of oceanic boundary currents, their separation, and numerical computation; additional laboratory experiments appear in Klinger (1993).

2. Narrow slope solutions

a. Western boundary step-up

The depth $h(y)$ of the slope in Fig. 2 equals H at $y = 0$ and increases to $H + \Delta H$ at $y = -W_*$. The latter is taken to be sufficiently small so that the separating streamline located at $\xi = \xi_s$ in the upstream flow $[U(\xi)]$ is located at $y = -y_0 < -W_*$ in the slope jet flow $u(y)$. As previously mentioned, we assume that the fraction $G = T_b/T_0$ of the upstream transport that crosses the slope displaces an equal amount ($T_c = T_b$) of (initially) resting shelf water back across the slope. In the steady laminar region, assumed farther downstream, this displaced water has the uniform potential vorticity $(f - u_y)/h(y) = f/H$. On the other side ($y \leq -y_0$) of the separating streamline, potential vorticity and mass conservation in this region of uniform depth are satisfied by making $u(y)$ in $y \leq -y_0$ *congruent* to $U(\xi)$ in $\xi > \xi_s$. Thus, corresponding velocities are equal, and the transports are equal, or

$$\int_{-\infty}^{-y_0} u(y)dy = \frac{T_d}{H + \Delta H} = \int_{\xi_s}^{\infty} U(\xi)d\xi, \quad (2.1)$$

$$u(-y_0) = U(\xi_s). \quad (2.2)$$

If $h(y)$ is a piecewise linear function of y, that is,

$$h(y) = H - sy \quad 0 \geq y \geq -W_*, \quad (2.3a)$$

$$s = \Delta H/W_* = \epsilon H/W_*, \quad \epsilon \equiv \Delta H/H, \quad (2.3b)$$

then the vorticity equation in $0 > y > -y_0$ becomes

$$-u_y = \begin{cases} -fsy/H, & 0 \geq y \geq -W_* \\ f\epsilon, & -W_* \geq y \geq -y_0, \end{cases}$$

and since $u(0) = 0$ the solution is

$$u(y) = \begin{cases} fsy^2/2H, & 0 \geq y \geq -W_* \\ u(-W_*) - f\epsilon(y + W_*), & -W_* \geq y_0 \geq -y_0. \end{cases} \quad (2.4b)$$

From the first of these equations and (2.3b) we obtain

$$u(-W_*) = f\epsilon W_*/2, \quad (2.5a)$$

and the second equation in (2.4b) then becomes

$$u(-y_0) = \epsilon f(y_0 - W_*/2), \quad (2.5b)$$

$$y_0 = \frac{u(-y_0)}{\epsilon f} + \frac{W_*}{2} = \frac{u(-y_0) + u(-W_*)}{\epsilon f}. \quad (2.5c)$$

Another equation connecting the unknowns y_0 and $u(-y_0)$ comes from the following consideration of the transport balance. When the entrained transport,

$$T_c = \frac{fs}{2H}\int_{-W_*}^{0} dyy^2H\left(1 - \frac{\epsilon y}{W_*}\right) + \frac{H + \Delta H}{2}[u(-W_*) + u(-y_0)](y_0 - W_*),$$

is simplified using (2.5a,c), the result is

$$T_c = \frac{f\epsilon HW_*^2}{8}\left(\frac{4}{3} + \epsilon\right) + \frac{H + \Delta H}{2\epsilon f}[u^2(-y_0) - u^2(-W_*)],$$

$$T_c = \frac{H + \Delta H}{2\epsilon f}u^2(-y_0) + \frac{(H + \Delta H)\epsilon fW_*^2}{24(1 + \epsilon)}. \quad (2.6)$$

The total transport $T_0 = \int_0^\infty d\xi U(\xi)$ is then obtained by adding (2.6) to T_d (2.1), and by using (2.2) we obtain the final result

$$\frac{U^2(\xi_s)}{2\epsilon f} + \frac{\epsilon fW_*^2}{24(1 + \epsilon)} = \int_0^{\xi_s} U(\xi)d\xi. \quad (2.7)$$

For any given $U(\xi)$ this can be solved for ξ_s, and G can then be obtained as the ratio of (2.7) to T_0.

This narrow slope solution is only valid if $y_0 > W_*$, where the value of y_0 obtained from (2.2), (2.5c) is

$$y_0 = \frac{U(\xi_s)}{\epsilon f} + \frac{W_*}{2},$$

and therefore the validity condition becomes

$$\frac{W_*}{2} < \frac{U(\xi_s)}{\epsilon f}. \quad (2.8)$$

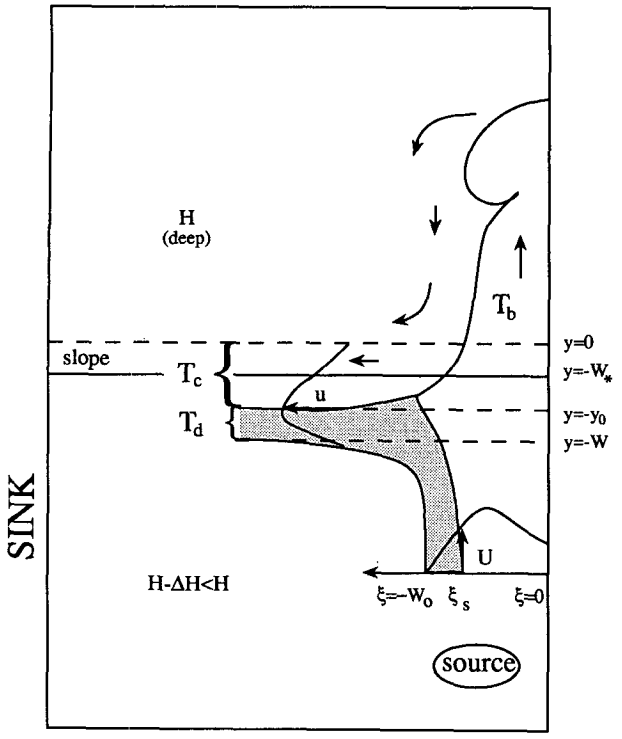

FIG. 3. The eastern boundary current [$U(\xi)$] version of Fig. 2 in which the current flows from a source on the shallow shelf into a deep downstream basin. As in the laboratory experiment, the sink is on the western wall of the shallow basin.

This is also *not* satisfied in the interesting case of a shallow shelf; that is, $H \to 0$, or $\epsilon = \Delta H/H \to \infty$, which will be discussed in the "wide" slope solution of section 3. When (2.8) is satisfied, the second term in (2.7) is an insignificant fraction ($1/12$) of the first term. A sketch of (2.7) for $U(0) = 0$ indicates one solution (ξ_s) if $U'(0)/f > \epsilon$, and otherwise there may be two (or no) solutions depending on the detailed $U(\xi)$.

b. *Eastern boundary step-down*

Although no new ideas appear in this geometry (Fig. 3), it is relevant to the experiment in section 5 and to the comparison with the theory of Spitz and Nof (1990), which did not take entrainment into account.

The following notation is the same as in subsection 2a, except that it is now convenient to denote the upstream depth by $H - \Delta H < H$, where H is the *downstream* depth, and

$$0 < \epsilon = \frac{\Delta H}{H} < 1.$$

The difference in the range of ϵ here and in section 2a is indicative of the significant dissimilarity between step-up and step-down topography. Our notational change makes the line by line derivation for the separating streamline ($\xi_s < 0$, in Fig. 3) almost identical (except for some sign changes) with section 2a, so that repetition is unnecessary, and the final result is

$$\frac{U^2(\xi_s)}{2\epsilon f} + \frac{\epsilon f W_*^2}{24(1-\epsilon)} = \int_{\xi_s}^{0} d\xi U(\xi), \ (\xi < 0) \quad (2.9)$$

$$y_0 = -\frac{u(-y_0)}{\epsilon f} + \frac{W_*}{2} = \frac{U(\xi_s)}{\epsilon f} + \frac{W_*}{2} > W_*, \quad (2.10)$$

$$\frac{W_*}{2} < \frac{U(\xi_s)}{\epsilon f}. \quad (2.10a)$$

A graphical sketch of the solution of (2.9) for ξ_s in Fig. 4a indicates that a bifurcated solution exists for all $U(\xi)$ if $W_*^2(1-\epsilon)^{-1}\epsilon f/24 \leq T_0$.

A more explicit result will be obtained for a triangular shaped $U(\xi)$ (Fig. 4b) whose inner width a is tentatively assumed to be smaller than the distance $|\xi_s|$ of the separating streamline from the wall. It is convenient to use $x \equiv W_0 + \xi$ as a new coordinate, where W_0 is the total width of $U(x)$. Then $U(0) = U(W_0) = 0$, and $U(x) = \zeta x$ in $0 \leq x \leq W_0 - a$, where ζ is the uniform vorticity in the cyclonic part of the upstream jet. Then (2.9) can be rewritten as

$$\frac{U^2(x_s)}{2\epsilon f} + f\omega^2 = \int_{x_s}^{W_0} dx U(x), \quad (2.11)$$

where

$$\omega^2 \equiv \frac{\epsilon W_*^2}{24(1-\epsilon)}. \quad (2.12)$$

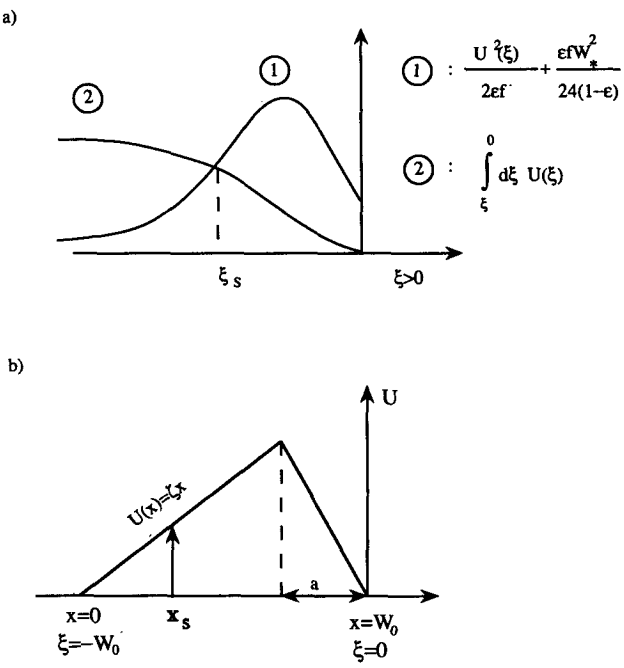

FIG. 4. (a) Sketch of the solution (2.9) for the separating streamline position ξ_s. (b) The triangular velocity profile used to compute $G = T_b/T_0$ in (2.15). The separating streamline is assumed (and subsequently verified) to be at $\xi = -x_s < -a < 0$.

Since $U(x_s) = \zeta x_s$, and since we assumed

$$a < W_0 - x_s, \tag{2.13}$$

then the value of the integral in (2.11) is

$$\tfrac{1}{2} W_0[\zeta(W_0 - a)] - \tfrac{1}{2} x_s[\zeta x_s].$$

Therefore, the solution of (2.11) is

$$x_s^2 = W_0(W_0 - a)\left[1 - \frac{2\omega^2 f/\zeta}{W_0(W_0 - a)}\right]\left(1 + \frac{\zeta}{\epsilon f}\right)^{-1}. \tag{2.14}$$

For sufficiently small W_* (or ω) $x_s^2 > 0$, and for sufficiently small a/W_0, the value of x_s is independent of a and still finite, so that (2.13) is satisfied; this verifies that the inner part of the upstream boundary current does not separate but continues into the downstream basin.

From (2.14) and $G = 1 - (T_0 - T_b)/T_0 = 1 - T_d/T_0$ we obtain

$$G = 1 - \frac{\frac{1}{2} x_s(\zeta x_s)}{\frac{1}{2} W_0[\zeta(W_0 - a)]},$$

$$G = \left[1 + \frac{2\omega^2 \epsilon f^2}{W_0(W_0 - a)\zeta^2}\right](1 + \epsilon f/\zeta)^{-1}. \tag{2.15}$$

$$G \geqslant \frac{1}{1 + \epsilon f/\zeta}. \tag{2.16}$$

The lower bound in (2.16) occurs when W_*, or (2.12), is sufficiently small so that the term containing ω^2 in (2.15) is negligible compared to unity, and this bound shows the expected decrease in cross-slope transport as the Rossby number (ζ/f) decreases and as ϵ increases. In general, however, G is expected to vary in a more complicated way, depending on the shape of $U(\xi)$.

The maximum $\epsilon = 1$ occurs for fixed $H - \Delta H$ when $H \to \infty$ and $\Delta H \to \infty$. These values and $a = 0$, $W_* = 0$ pertain to the simple half-jet model of Spitz and Nof

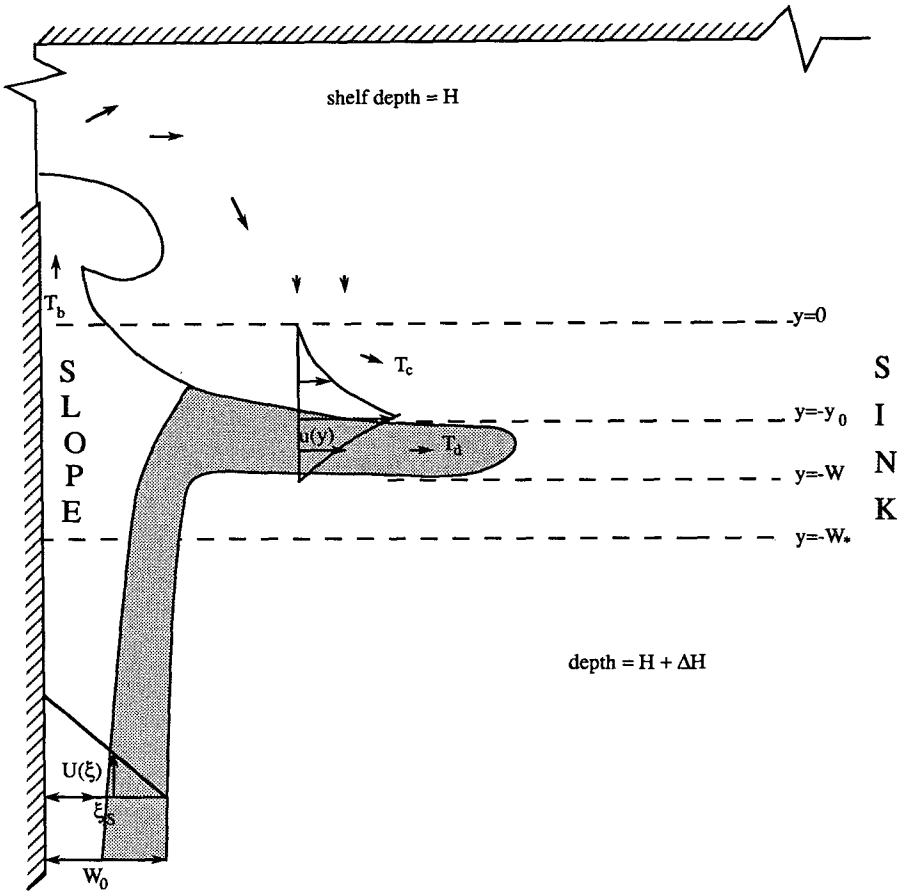

FIG. 5. The wide slope model in which the entrained transport T_c lies entirely on the slope. The calculation (section 3) is for an upstream current with uniform relative vorticity.

(1990); they also assume that no part of their upstream current crosses the escarpment ($G = 0$) and that the velocity discontinuity [in $u(y)$] exists there. In our Eq. (2.12), $\epsilon \to 1$ with $W_* \to 0$ gives a singular limit, but there is a parametric range $W_*^2 \leqslant O(1 - \epsilon)$, where ω is finite, and consequently $G > 0$ in (2.15). Although the wall velocities must be vanishingly small in the deep ($H \to \infty$) downstream basin, we conclude that the volume transport is finite, and this produces a *finite counterflow across the escarpment,* where it is entrained.

3. Wide continental shelf, western boundary step-up

The solution (2.7) is inapplicable when (2.8) is not satisfied, and this may occur either when W_* becomes large, or when the shelf depth (H) becomes small. In that case the amount of entrained water is so small that no part of it is able to cross the *entire* slope, and all of it is confined to a region near the top, as sketched in Fig. 5. We shall show that the small volume of entrained shelf water forms an "inertial boundary layer" whose large cyclonic vorticity enables the velocity to vanish on the inshore side of the continental slope; herein lies the oceanographic interest in this case.

For simplicity the following analysis is again restricted to an upstream half jet $U(\xi) = \zeta(W_0 - \xi)$ with uniform anticyclonic vorticity ζ in $0 < \xi < W_0$. The slope width W_* is now assumed to be sufficiently large so that not only the separating streamline ($y = -y_0 > -W_*$) but also the entire bifurcating branch ($-y_0 > y > -W$) lies *entirely* on the slope (Fig. 5). This branch is therefore no longer congruent to $U(\xi)$, because of the topographic modification of its vorticity. The slope depth $h(y)$ is again taken to be linear in $y < 0$; that is,

$$h(y) = H + \Delta h(y), \quad \Delta h(y) = -sy, \qquad s = \frac{\Delta H}{W_*} < \frac{\Delta H}{W} \tag{3.1}$$

so that the relative vorticity of the entrained fluid in $0 > y > -y_0$ is $-fsy/H$ and the velocity is again given by

$$u(y) = \frac{fsy^2}{2H}. \tag{3.2}$$

In the region $y < -y_0$ of uniform potential vorticity $(f - \zeta)/(H + \Delta H)$, the relative vorticity is

$$-\frac{\partial u}{\partial y} = \frac{H + \Delta h(y)}{H + \Delta H}(f - \zeta) - f. \tag{3.3a}$$

Since no velocity discontinuity is permitted in our piecewise uniform potential vorticity model, $u(-W) = 0$ is the boundary condition, and (3.3a) yields

$$u(y) = \frac{f\Delta H + \zeta H}{H + \Delta H}(y + W) + \frac{s(f - \zeta)(y^2 - W^2)}{2(H + \Delta H)}. \tag{3.3b}$$

The equality of (3.3b) and (3.2) at $y = -y_0$ gives one equation

$$\frac{fsy_0^2}{2H} = \frac{(f\Delta H + \zeta H)}{H + \Delta H}(W - y_0) - \frac{s}{2}\frac{(f - \zeta)}{H + \Delta H}(W^2 - y_0^2)$$

for the two unknowns (y_0, W), and when this equation is simplified using the nondimensional quantities,

$$\eta = y_0/W, \quad \kappa = 2H/sW, \tag{3.4a}$$

$$R = \zeta/f, \quad \epsilon = \Delta H/H, \tag{3.4b}$$

we obtain

$$2\eta = -\kappa + [\kappa^2 + 4(\kappa - (1 - R)(\epsilon + R)^{-1})]^{1/2}. \tag{3.5}$$

A second equation relating the two unknowns comes from the transport relation $T_0 = T_c + T_d$, where

$$\frac{T_c}{f} = \int_{-y_0}^{0} dy(H - sy)sy^2/2 \tag{3.6}$$

$$\frac{T_d}{f} = \frac{1}{f}\int_{-W}^{-y_0} dy(H - sy)\left[\frac{f\Delta H + \zeta H}{H + \Delta H}(y + W) + \frac{s(f - \zeta)(y^2 - W^2)}{2(H + \Delta H)}\right]. \tag{3.7}$$

When these integrals are computed and nondimensionalized, the transport relation becomes

$$\frac{T_0}{f} = \frac{sW^3}{2}\left(\frac{\eta^3}{3} + \frac{\eta^4}{2\kappa}\right) + \frac{(\epsilon + R)HW^2}{1 + \epsilon}\left[Z + \left(1 - \frac{2}{\kappa}\right)\frac{Z^2}{2} - \frac{2}{3}\frac{Z^3}{\kappa}\right]_{-1}^{-\eta} + \frac{s(1 - R)W^3}{2(1 + \epsilon)}\left[-Z + \frac{Z^2}{2} + \frac{Z^3}{3} - \frac{Z^4}{\kappa}\right]_{-1}^{-\eta}, \tag{3.8}$$

where it is understood here that the bracketed quantity evaluated at $Z = -\eta$ is to be subtracted from its value at $Z = -1$. Equations (3.5), (3.8) determine η, κ (or y_0, W), and $G = T_b/T_0 = T_c/T_0$.

Rather than give a complete discussion of the result, attention is directed to the interesting $H \to 0$ limit, with fixed W_*, s, and R. Then (3.4a,b) give $\kappa \to 0$, $\epsilon \to \infty$, and the limit of (4.5) is $\eta \to [\kappa - (1 - R)/\epsilon]^{1/2}$ or

$$\frac{y_0}{W} = \eta = \left(\frac{2H}{sW}\right)^{1/2}\left(1 - \frac{(1 - R)W}{2W_*}\right)^{1/2} \to 0. \tag{3.9}$$

Since $W < W_*$ (Fig. 5), it follows that $y_0 = O(H^{1/2}) \to 0$, and $h(-y_0) - H = O(H^{1/2})$. Since this is still much larger than $h(0) = H$, it follows that a very large $(fH^{-1/2})$ cyclonic shear exists within the small interval

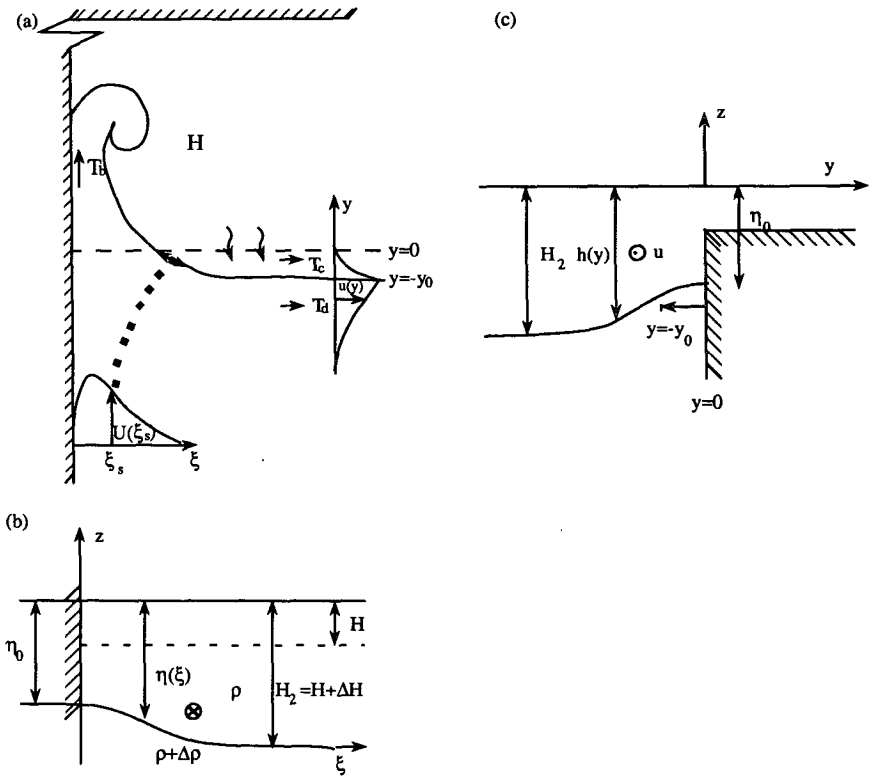

FIG. 6. Bifurcation and entrainment in the upper layer of a two-layer fluid in which the dense bottom layer is deep and resting. The calculations (section 4) are for a "very narrow" slope width, here shown as a discontinuity at $y = 0$. (a) Top view of current profiles. (b) Vertical section upstream showing the upper-layer fluid of density ρ. (c) Vertical section of bifurcated jet looking upstream.

$0 > y > -y_0$. With the exception of this novel kind of *inertial boundary layer,* the flow along the northern boundary is the same as would occur if $h(0) = 0$ (i.e., no shelf). It is the small amount of entrained fluid, however, that brings the inshore velocity $[u(y)]$ to zero on the shelf of finite depth. It would be interesting to see the influence of this shelf on a simple barotropic model of a global ocean circulation model.

If the value of W computed above is not less than W_*, a third case arises in which part of the bifurcated current lies in the deep basin $(H + \Delta H)$, and part lies on the slope. The former has vorticity $-\zeta$, the latter has vorticity (3.3a), and Eq. (3.2) is still the velocity in the entrained cyclonic layer $0 > y > -y_0$. The three layers must be joined by equating velocities at their edges, and it seems reasonably clear that when $H \to 0$ a cyclonic inertial boundary layer will still appear.

4. Baroclinic bifurcation

To illustrate the generalizability of the entrainment effect to baroclinic boundary currents we shall briefly consider the simplest case of a $1\frac{1}{2}$-layer model (Fig. 6). In addition, the width of the continental slope at $y = 0$ is assumed to be very narrow (cf. $W_* \to 0$ in section 2), and the shelf depth H is assumed to be less than the minimum upstream thickness (η_0) of the upper layer, which has density ρ and velocity $U(\xi)$. The underlying water of density $\rho + \Delta\rho$ is assumed to be at rest, so that the upstream geostrophic balance requires $U(\xi) = (g^*/f)\partial\eta/\partial\xi$, where $g^* = g\Delta\rho/\rho$ and $\eta(\xi)$ is the layer thickness. A fraction $G = T_b/T_0$ of the light fluid continues along the wall and into the shelf, where it displaces an equal volume $(T_c = T_b)$ of initially resting shelf water as a countercurrent across $y = 0$. The high potential vorticity columns stretch and merge at $y = -y_0$ with the bifurcated current (T_d) to form a steady laminar jet $u(y) = -g^*/f\partial h/\partial y$, with $u = 0$ for $y \geq 0$.

If $\xi = \xi_s$ denotes the upstream position of the separating streamline passing through $y = -y_0$, then mass and potential vorticity conservation are satisfied if $\eta(\xi)$ in $\xi > \xi_s$ is congruent to $h(y)$ in $y < -y_0$, and therefore

$$\eta(\xi_s) = h(-y_0), \quad U(\xi_s) = u(-y_0). \tag{4.1}$$

Since only finite vorticity can be generated in Fig. 6, the geostrophic velocity $u = -(g^*)(f)\partial h/\partial y$ is con-

tinuous across $y = 0$, and since $u = 0$ for $y > 0$, we obtain

$$\frac{\partial h(0-)}{\partial y} = 0, \tag{4.2}$$

as one boundary condition. The second one

$$h(0) = \eta_0 \tag{4.3}$$

follows from the equality of the total upstream geostrophic transport $g^*/2f(H_2^2 - \eta_0^2)$ and the total transport $g^*/2f[H_2^2 - h^2(0)]$ of $u(y)$.

In the region $0 \geq y \geq -y_0$ of uniform potential vorticity $[(f - du/dy)/h(y) = f/H]$, we have

$$\frac{d^2h}{dy^2} - \frac{f^2h}{g^*H} = -\frac{f^2}{g^*}, \tag{4.4}$$

and the solution satisfying (4.2), (4.3) is

$$h(y) = H + (-H + \eta_0)\cosh(y/\lambda), \tag{4.5a}$$

$$u(y) = -\frac{g^*}{f\lambda}(-H + \eta_0)\sinh(y/\lambda), \tag{4.5b}$$

$$\lambda = (g^*H/f^2)^{1/2}. \tag{4.5c}$$

The matching conditions (4.1) then yield

$$\eta(\xi_s) = H + (-H + \eta_0)a, \tag{4.6a}$$

$$U(\xi_s) = \frac{g^*}{f\lambda}(-H + \eta_0)(a^2 - 1)^{1/2}, \tag{4.6b}$$

where

$$a = \cosh(y_0/\lambda). \tag{4.6c}$$

Elimination of a gives a single equation,

$$U^2(\xi_s) = \left[\frac{g^*(-H + \eta_0)}{f\lambda}\right]^2\left[\left(\frac{\eta(\xi_s) - H}{\eta_0 - H}\right)^2 - 1\right], \tag{4.7a}$$

for ξ_s in terms of the given upstream state $U(\xi) = g^*/fd\eta/d\xi$. The fraction ($G = T_c/T_0$) of the total transport flowing on the shelf can then be computed from

$$G = \frac{\eta^2(\xi_s) - \eta_0^2}{H_2^2 - \eta_0^2}. \tag{4.7b}$$

For further discussion we consider an upstream flow with uniform potential vorticity f/H_2, in which case

$$\eta(\xi) = H_2 - (H_2 - \eta_0)e^{-\xi/\lambda_2}, \tag{4.8a}$$

$$U(\xi) = \frac{g^*(H_2 - \eta_0)}{(g^*H_2)^{1/2}}e^{-\xi/\lambda_2}, \tag{4.8b}$$

$$U(\xi_s) = \frac{g^*[H_2 - \eta(\xi_s)]}{(g^*H_2)^{1/2}}, \tag{4.8c}$$

$$\lambda_2 = \left(\frac{g^*H_2}{f^2}\right)^{1/2}. \tag{4.8d}$$

Instead of solving (4.7) for ξ_s it is simpler to use (4.8c) to eliminate $U(\xi_s)$ and to use (4.6a) to eliminate $\eta(\xi_s)$. The resulting equation for a or for the separating streamline (i.e., y_0) is

$$\frac{H_2}{H}(-H + \eta_0)^2(a^2 - 1) = [H_2 - H - a(-H + \eta_0)]^2. \tag{4.9}$$

As in the barotropic problem, the solution for the shallow shelf ($H/\eta_0 \ll 1$) is of particular interest and, when $H \to 0$, Eq. (5.9) requires $a \to 1$. When the power series

$$a = 1 + \alpha(H/\eta_0) + \cdots O(H/\eta_0)^2 \tag{4.10}$$

is substituted into (4.9), the leading terms in the expansion give

$$\alpha = \frac{1}{2}\left(\frac{H_2}{\eta_0} + \frac{\eta_0}{H_2}\right) - 1. \tag{4.11}$$

By substituting this and

$$a - 1 = \cosh(y_0/\lambda) - 1 = \frac{y_0^2f^2}{2g^*H} + \cdots$$

into (4.10), we get the asymptotic solution

$$\frac{y_0}{(g^*\eta_0/f^2)^{1/2}} = \frac{H}{\eta_0}(H_2 - \eta_0)(H_2\eta_0)^{-1/2} + \cdots O(H/\eta_0)^2 \tag{4.12}$$

for the small thickness $y_0 = O(H)$ of the cyclonic inertial boundary layer. Inside this layer Eq. (4.5b) gives

$$-\frac{\partial u}{\partial y} \to \frac{g^*\eta_0}{f\lambda^2} = \frac{\eta_0}{H}f \to \infty. \tag{4.13}$$

This demonstrates the large shear that can be generated on the inshore side of the free jet.

5. Laboratory experiment on eastern boundary step-down

The source–sink laboratory experiment (Figs. 7a, 8) used to test the qualitative entrainment assumption consisted of an "inner" tank (53 × 53 cm) containing a Plexiglass shelf (16.5 cm wide) and a slope (17 cm wide), tape-hinged together so that different ΔH values could be easily obtained. A spillway on the western side of the shallow *shelf* served as a distributed sink for the overflow into an "outer" tank, and this provided a constant free-surface height ($H = 20$ cm) for the working fluid. Without this sink the slowly rising water level produced unwanted large-scale gyres on the shelf and in deep water, but with the sink the *net* flux of water across the shelf and into the deep semienclosed basin in Fig. 8 vanishes at all times. The eastern boundary current emerged from a 3.5-cm wide sandstone and glass block (originally designed as an air diffuser for

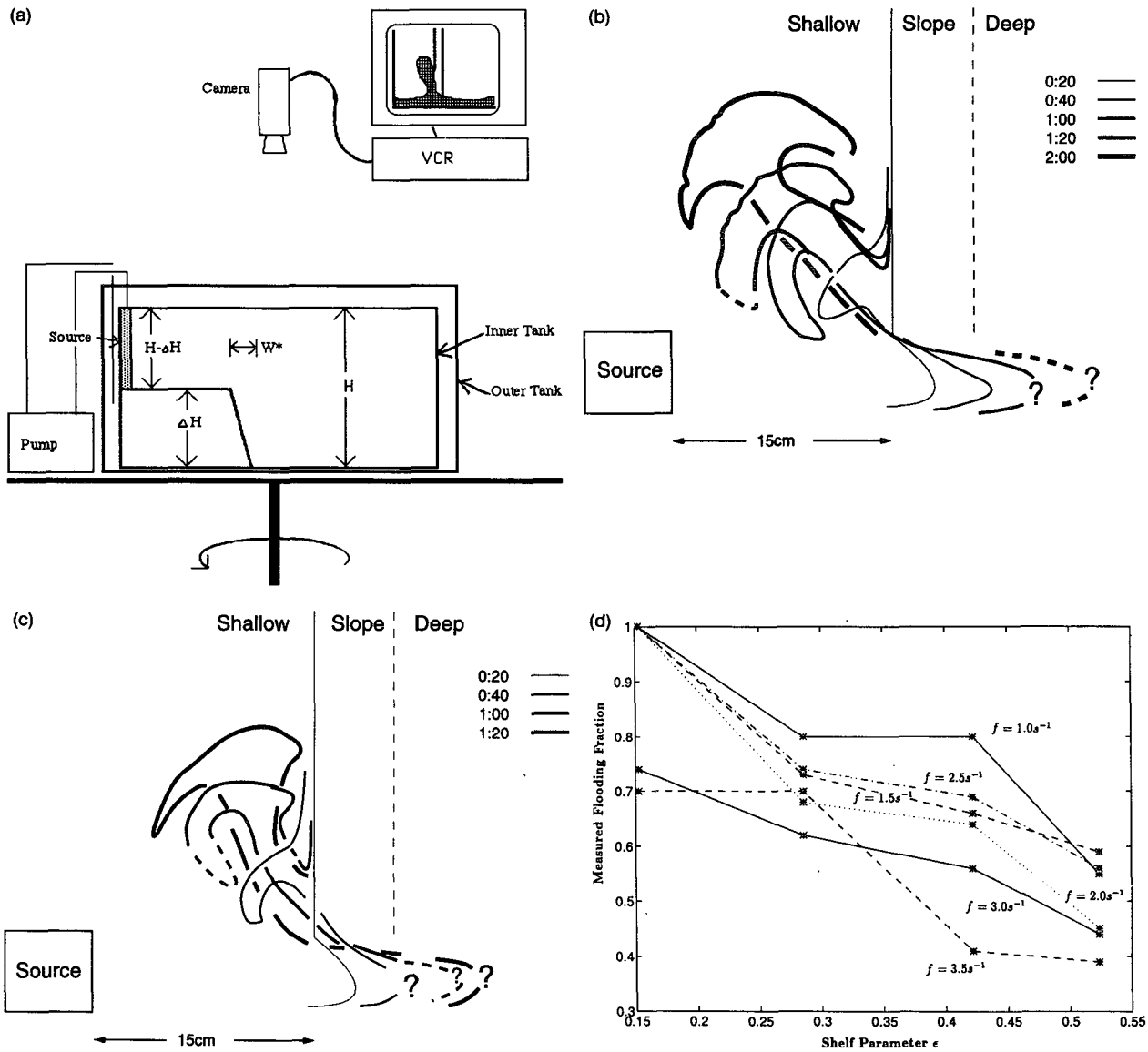

FIG. 7. (a) Schematic diagram of the experiment for the runs in Table 1, showing the dyed (stipled) fluid emerging from a source on the "eastern" wall of an inner tank. A free overflow (distributed sink) occurs on the wall of this, which is located at the western boundary shelf. (b) Hand-drawn tracings from the video screen of a thymol blue line emitted from a wire electrode placed along and above the top of the slope in run 56 with $\epsilon = 0.52, f = 1.5\ s^{-1}$; the times are 20 s, 40 s, 1 min, 1 min 20 s after the source flow was initiated. The dye lines reveal the entrance of the wall jet into deep water and the adjacent countercurrent of deep water flowing onto the shelf; westward of this the dye line remains undeflected. The question marks and dashed lines indicate diffuse and hard to locate portions of the dye. (c) Same as (b) except for $f = 2.5\ s^{-1}$ (run 57). The tank geometry in Figs. 5b,c differs from the main runs (Table 1, Fig. 8) insofar as the sink occurs along the *entire* western wall. (d) The flooding fraction F_Q (5.1) obtained from Table 1 is plotted for six different rotation rates as a function of ϵ.

fish tanks), which was covered with metal tapes on three sides in order to force the current out on the side facing the slope. A continuous closed circuit flow of distilled water from the sink (outer tank) to the source was maintained by a peristaltic pump (an ordinary pump introduced temperature variations sufficient to produce nonbarotropic flow). The thymol blue technique was used to dye the flow emerging from the source (Fig. 8) and also to produce thin dye lines (Figs. 7b,c) from wire electrodes strung across various parts and depths of the tank. This dye marking procedure enabled us to verify the barotropic structure and to determine how entrainment into the bifurcated jet occurred. The entire apparatus was covered with Plexiglas and photographed from above by a zoom lens camera whose video tapes could be subsequently analyzed.

Although the source discharge was kept constant, the jet on the shelf contained strong two-dimensional dis-

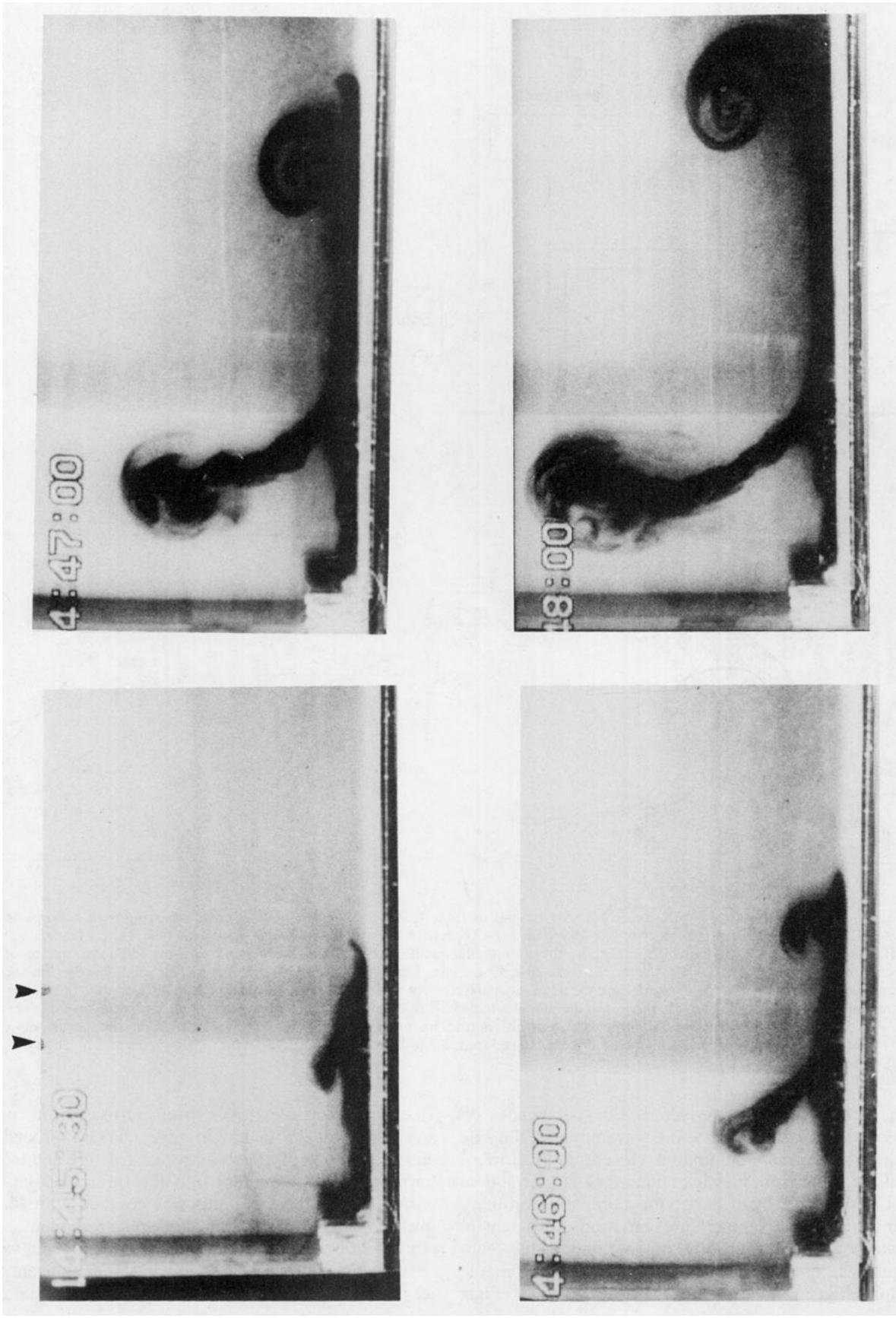
47:00
48:00
48:00

turbances (obscured in Fig. 8 because of the dye); these are similar to the eddies in the flat-bottom experiment of Stern and Whitehead (1990), but they intensify on crossing the slope. Thirty seconds after starting the pump (the first frame in Fig. 8), the leading edge of the wall current has just passed the slope and entered the deep basin; the developing bifurcation can be seen in the countercurrent emerging from the shelf break. The next frame shows more clearly the dyed part of the bifurcating free jet inclined at a small angle relative to the shelf break. Meanwhile, the nose of the wall current propagates into the deep basin with decreasing speed, and in some runs it appears to stagnate before reaching the "north" wall, suggesting that dissipative effects are important in this region (see the conclusions).

Dye lines (such as those traced in Figs. 7b,c) emitted from the wire electrodes confirmed the foregoing picture by revealing both the wall current and the adjacent countercurrent. The latter clearly emerges from the deeper regions, crosses the slope, and enters the shelf, where it merges with the bifurcated current (see Fig. 8). This strong countercurrent is one of two possible ways in which the mass budget of the semienclosed deep basin can be satisfied, the other way being by a broad and weak current extending over the *entire* slope; but there was no indication of the latter in careful visual observations of the dye line patterns. One reason seems to be that the large ΔH precludes a *weak* flow across the isobaths. On the other hand, the narrow counterflow might be continually generated at the base of the slope by the potential vorticity front at the leading edge of successive eddies embedded in the wall current; each one of these might produce a displacement similar to the "nose" in Fig. 3. The curves in Figs. 7b,c are tracings of the dye lines on the video screen recorded in earlier runs than in Table 1, where the conditions were similar, except that the wall was of uniform height along the entire western boundary, so that a possible sink existed in the deep basin as well as in the shallow one (Table 1). But the qualitative nature of the thymol blue lines was the same in all of our runs.

Although the experiment was not designed to obtain quantitative velocities, a qualitative measure of the relative flux of fluid across the slope was obtained as follows. The visible areas and the volumes $Q_{\text{deep}}(t)$, $Q_{\text{shelf}}(t)$ of the dyed fluid in each basin (Fig. 8) were measured from planimetered traces of the continuous videotape. Volumes obtained every minute for a minimum of 3 min (which was approximately the time for the eastern boundary current to reach the north wall) were fitted by regression lines, which determined a "flooding fraction":

$$F_Q = \frac{\dot{Q}_{\text{deep}}}{\dot{Q}_{\text{deep}} + \dot{Q}_{\text{shelf}}}, \tag{5.1}$$

where the dot indicates a time derivative. These $\dot{Q}$ differ substantially from the volume fluxes (T) because eddy diffusion in each branch increases the visible dye volume. (At the end of one complete run the total visible volume of dye was four times the total volume flux!) Nevertheless, the diffusion rate should have some correlation with the volume flux rate, and the values of (5.1) in Table 1 provide a qualitative measure of the bifurcation. Although a detailed comparison of F_Q with (2.15) is unwarranted, the bound (2.16) is listed in the last column of Table 1 and is seen to be systematically lower than F_Q. The plot of all F_Q (Fig. 7d) reflects the expected decrease of cross-slope transport with increasing topography (ϵ). In all of the runs (Table 1) the source flow rate (T_0), the distance (15 cm) of the source from the shelf break, and the free-surface height ($H = 20$ cm) were held constant; the only variable parameters were f, ϵ, $H - \Delta H$, and the horizontal extent W_* of the slope. The "maximum" jet velocity U_0 was determined from the average propagation of the dyed nose (Fig. 8) on the shelf, and a nominal width W_0 was determined from U_0, $H - \Delta H$, and T_0 for an assumed parabolic velocity profile, rather than from the highly variable dye widths. Perhaps the most significant quantitative conclusion from Table 1 occurs for the group of four points ($\epsilon = 0.15$) for which $F_Q = 1$ and for which it is certain that *all* of the wall current enters the deep basin. These points correspond to the smallest ϵ in the group, which supports the earlier suggestion of nonunique statistically steady states and the existence of threshold values of (ϵ, f) below which the realized current remains entirely on the wall, that is, *no* bifurcation occurs.

We also note that the entire bifurcated jet in Fig. 8 drifts onto the shelf, where the depth is uniform, whereas in the theory (Fig. 3) part of the jet lies on the topographic slope. Although the theory could be made to conform with this observation by setting $u(-W_*) = 0$ in Fig. 3 and re-solving, such an ad hoc adjustment seems unwarranted because other physical effects, such as Ekman friction, are probably responsible for the downstream evolution of the jet on the shelf in Fig. 8.

FIG. 8. The thymol blue dyed current emerging from a source on the shelf of the eastern boundary and flowing toward a slope (indicated by the two arrowhead markings on the first frame). Run 72, $\epsilon = 0.42, f = 2.05^{-1}$; see Table 1. The first frame (top, left) is at $t = 30$ s after initiating the flow; the next two are at 60 and 120 s, respectively, and the frame on the bottom right is at $t = 180$ s. The bifurcating jet contains water originating in the deep basin (as well as directly from the source) as is verified by the dye line tracings (Figs. 7b,c). The boundary current on the wall contains two-dimensional disturbances that are masked by the dye, but are revealed by other techniques (not shown here).

TABLE 1. Experimental conditions for runs in which the sink was confined to the western wall of the shelf. The symbol F_Q is the volume fraction of the dye (Fig. 8) that occupies the deep basin after flowing across the slope (see text). The last column is the estimated lower bound (2.16) for G.

Run no.	Shelf height (cm)	W_* Slope width (cm)	ϵ	f (s)$^{-1}$	Flow rate (ml s)$^{-1}$	F_Q	U_0 (cm s)$^{-1}$	W_0 Current width (cm)	$\left(1+\frac{\epsilon f W_0}{2U_0}\right)^{-1}$
64	5.8	2.0	0.28	2.5	5.7	0.74	0.50	2.5	.36
65	5.8	2.0	0.28	3.0	5.7	0.62	0.36	2.5	.26
66	5.8	2.0	0.28	3.5	5.7	0.70	0.33	2.5	.21
67	5.8	2.0	0.28	2.0	5.7	0.68	0.36	1.5	.46
68	5.8	2.0	0.28	1.5	5.7	0.73	0.43	1.5	.58
69	5.8	2.0	0.28	1.0	5.7	0.80	0.40	2.0	.59
70	8.6	3.5	0.42	1.0	5.7	0.80	0.68	1.5	.68
71	8.6	3.5	0.42	1.5	5.7	0.66	0.72	1.5	.60
72	8.6	3.5	0.42	2.0	5.7	0.64	0.72	1.5	.53
73	8.6	3.5	0.42	2.5	5.7	0.69	0.56	1.7	.39
74	8.6	3.5	0.42	3.0	5.7	0.56	0.68	2.0	.35
75	8.6	3.5	0.42	3.5	5.7	0.41	0.61	1.5	.36
76	10.6	4.0	0.52	1.0	5.7	0.55	0.61	4.0	.38
77	10.6	4.0	0.52	1.5	5.7	0.80	0.72	2.0	.48
78	10.6	4.0	0.52	2.0	5.7	0.45	0.72	2.0	.41
79	10.6	4.0	0.52	2.5	5.7	0.56	0.72	2.0	.36
80	10.6	4.0	0.52	3.0	5.7	0.44	0.76	2.0	.33
81	10.6	4.0	0.52	3.5	5.7	0.39	0.65	2.5	.22
82	3.1	0.8	0.15	1.0	5.7	1.00	0.29	2.0	.66
83	3.1	0.8	0.15	1.5	5.7	1.00	0.29	1.5	.63
84	3.1	0.8	0.15	2.0	5.7	1.00	0.27	1.5	.55
85	3.1	0.8	0.15	2.5	5.7	1.00	0.27	1.5	.49
86	3.1	0.8	0.15	3.0	5.7	0.74	0.26	1.5	.44
87	3.1	0.8	0.15	3.5	5.7	0.70	0.27	1.3	.44
88	3.1	0.8	0.15	4.0	5.7	0.65	0.24	1.5	.35

The main purpose of the experiment has been served by merely confirming the kinematical picture of the bifurcation and entrainment.

6. Conclusions

The bifurcation process discussed herein is one way in which a western boundary current can generate large inshore shear by entraining high potential vorticity water on the continental slope or shelf. This idea is supported by a qualitative laboratory experiment and by a steady-state barotropic model whose topographic variation is sufficient to ensure that at least some of the upstream current follows the slope isobaths. These studies show that the inshore flow that enters the downstream basin displaces a narrow countercurrent across the isobaths, where it merges with the bifurcated branch of the upstream flow.

For an arbitrary upstream current $U(\xi)$ incident on a narrow shelf the location (ξ_s) of the separating streamline is given by (2.7) or (2.9), and this determines the transport fraction G crossing the slope. Part of the upstream current always remains on the wall [(2.13)–(2.15)], unlike the situation in classical boundary layer separation at a curved wall. The interesting feature emphasized in the wide slope model (section 3) and the baroclinic model (section 4) is the large shear in the inshore inertial boundary layer associated with a shallow shelf.

The main qualitative aspects of separation, bifurcation, and entrainment are revealed by dye observations in the source–sink experiment. These show (Fig. 8) a branch of the upstream current separating from the wall near the slope, and our visual observations of the thymol blue dye lines emitted from wire electrodes show (Figs. 7b,c) that the entrained countercurrent emerges from the downstream edge of the slope and then flows cross slope into the upstream basin. From the videotapes it appears that this countercurrent is either statistically steady or slowly varying and is forced by the potential vorticity front at the leading edge of eddies in the wall current as they intensify on the slope and propagate downstream (where they ultimately decay).

Of the many differences between the experiment and the theory, the most accessible one is the $F_Q = 1$ dye observations (runs 82–85 in Table 1) that unambiguously indicate finite threshold values of (f, ΔH) below which bifurcation is *not* realized ($G = 1$). This is related to the apparent nonuniqueness of the class of steady solutions; it is a simple matter to obtain a downstream solution on the wall with $G = 1$ (no bifurcation). But the interesting theoretical problem is the determination of the critical value of (f, ΔH) at which some bifurcation occurs. This ques-

tion, as well as others related to the validity of our qualitative assumptions (e.g., Fig. 1), might be addressed by extending contour dynamical initial value calculation of the intrusion of a semiinfinite wall jet (Stern and Pratt 1985) using the Green's functions appropriate to a piecewise uniform topography (Bidlot and Stern 1994).

Acknowledgments. We thank Dr. Jack Whitehead (WHOI) for providing the experimental facilities. An NSF graduate assistantship is acknowledged by JA, and NSF also supplied partial support for MES during a GFD summer program.

REFERENCES

Bidlot, J. R., and M. E. Stern, 1994: Maintenance of continental boundary shear through countergradient vorticity flux in a barotropic model. *J. Fluid Mech.*, **271,** 55–85.

Hsueh, Y., J. Wang, and C.-S. Chern, 1992: The intrusion of the Kuroshio across the continental shelf northeast of Taiwan. *J. Geophys. Res.*, **97**(C9), 14 323–14 303.

Ierly, G. R., 1990: Boundary layers in the general ocean circulation. *Annu. Rev. Fluid Mech.*, **22,** 111–142.

Johnson, E. R., 1985: Topographic waves and the evolution of coastal currents. *J. Fluid Mech.*, **160,** 499–509.

Klinger, B. A., 1993: Gyre formation at a corner by rotating barotropic coastal flows along a slope. *Dyn. Atmos. Oceans,* **19,** 27–63.

Munk, W., 1950: On the wind driven circulation. *J. Meteor.*, **7,** 79–93.

Spitz, Y. H., and D. Nof, 1990: Separation of boundary currents due to bottom topography. *Deep-Sea Res.*, **38,** 1–20.

Stern, M. E., 1991: Countergradient vorticity flux generated in continental boundary currents. *J. Phys. Oceanogr.*, **21,** 1622–1630.

——, and L. J. Pratt, 1985: Dynamics of vorticity fronts. *J. Fluid Mech.*, **161,** 513–532.

——, and J. A. Whitehead, 1990: Separation of a boundary jet in a rotating fluid. *J. Fluid Mech.*, **217,** 41.

Warren, B. A., 1969: Divergence as a cause of current branching. *Deep-Sea Res.*, **16** (Suppl.), 339–355.